Rare Met. (2019) 38(6):552–560
https://doi.org/10.1007/s12598-019-01225-2

RARE METALS
www.editorialmanager.com/rmet

Antibacterial ability and cytocompatibility of Cu-incorporated Ni–Ti–O nanopores on NiTi alloy

Jia-Ming Zhang, Yong-Hua Sun, Ya Zhao, Yan-Lian Liu, Xiao-Hong Yao, Bin Tang, Rui-Qiang Hang*

Received: 10 December 2018 / Revised: 24 December 2018 / Accepted: 28 January 2019 / Published online: 14 March 2019

Abstract Nearly equiatomic nickel–titanium (NiTi) alloy is an ideal implant biomaterial because of its shape memory effect, superelasticity, low elastic modulus as well as other desirable properties. However, it is prone to infection because of its poor antibacterial ability. The present work incorporated Cu into Ni–Ti–O nanopores (NP–Cu) anodically grown on the NiTi alloy to enhance its antibacterial ability, which was realized through electrodeposition. Our results show that incorporation of Cu (0.78 at%–2.37 at%) has little influence on the NP diameter, length and morphology. The release level of Cu ions is in line with loadage which may be responsible for the improved antibacterial ability of the NiTi alloy to combat possible bacterial infection in vivo. Meanwhile, the NP–Cu shows better cytocompatibility and even can promote proliferation of bone marrow mesenchymal stem cells (BMSCs), up-regulate collagen secretion and extracellular matrix mineralization when compared with Cu-free sample. Better antibacterial ability and cytocompatibility of the NP–Cu render them to be promising when serving as NiTi implant coatings.

Keywords Nickel–titanium alloy; Nickel–titanium–oxygen nanopores; Copper; Antibacterial ability; Cytocompatibility

J.-M. Zhang, Y.-H. Sun, Y. Zhao, Y.-L. Liu, X.-H. Yao, B. Tang, R.-Q. Hang*
Research Institute of Surface Engineering, College of Materials Science and Technology, Taiyuan University of Technology, Taiyuan 030024, China
e-mail: hangruiqiang@tyut.edu.cn

1 Introduction

Nearly equiatomic nickel–titanium (NiTi) alloy has been extensively used as an orthopedic and orthodontic implant material due to its desirable properties, such as unique shape memory effect, superelasticity, low elastic modulus and high corrosion resistance [1–4]. However, infection is an inevitably potential risk for all kinds of biomaterials including the NiTi alloy [5]. It may result in patient suffering, financial burden and even fatality [6, 7]. Therefore, improving the antibacterial ability of the alloy is highly required.

Surface modification is a feasible and economic approach to endow the NiTi alloy with good antibacterial ability without compromising its desirable bulk attributes. Recently, ordered nickel–titanium–oxygen (Ni–Ti–O) nanopores (NPs) with proper length anodically grown on the NiTi alloy show good cytocompatibility [8–10]. Our recent work also demonstrates that Ni–Ti–O NPs exhibit antibacterial ability through releasing Ni ions [10], but in some harsh conditions, the antibacterial ability is relatively poor. In addition, excessive release of Ni ions may raise safety concerns because it is reported that Ni is toxic and even carcinogenic to human beings [11]. In order to solve the problem, shortening NPs to minimize Ni release and incorporating more potent and safer antibacterial agent may be a feasible way. Inorganic antibacterial agents such as silver (Ag) [12, 13], copper (Cu) [14, 15] and zinc (Zn) [16, 17] have been incorporated into the implant surfaces to endow them with good antibacterial ability. Among them, Cu exhibits desirable antibacterial properties against numerous bacteria strains [18, 19] and provides better compromise between antibacterial effectiveness and cytotoxicity compared with Zn and Ag [20]. More importantly,

Cu is one of the essential trace elements required for human beings and takes part in synthesis and release of life-sustaining proteins and enzymes within the living organisms [14]. Collectively, it may be a highly desirable choice to incorporate Cu into Ni–Ti–O NPs in order to well balance antibacterial ability and cytocompatibility of NiTi-based implants to meet better clinical needs.

In the present work, Ni–Ti–O NPs were firstly fabricated on the NiTi alloy by anodization, followed by incorporation of Cu into NPs by electrodeposition. Then, Ni and Cu ions release, antibacterial ability and cytocompatibility of the samples were investigated.

2 Experimental

2.1 Preparation of Cu-incorporated Ni–Ti–O nanopores

Commercial NiTi alloy (50.8 at% Ni) rod with 12 mm in diameter (Xi'an SaiTe Metal Materials Development Co., Ltd., China) was cut into small pieces (2.5 mm in thickness), which were then ground, mirror-polished and used as substrates. All the samples were ultrasonically cleaned with acetone, ethanol and deionized water sequentially followed by drying in air. The Ni–Ti–O NPs were fabricated by anodization of the NiTi alloy sheet in an ethylene glycol electrolyte containing 5.0 vol% H_2O and 0.3 mol·L^{-1} NaCl at 10 V for 5 min. Anodization was carried out in a two-electrode setup with Pt sheet as the counter electrode and the sample as the working electrode. After anodization, the prepared samples were immediately ultrasonically cleaned in deionized water to remove the remaining electrolyte as well as the undesired irregular oxide layers on their surfaces.

Electrodeposition was carried out on an electrochemical workstation (CHI660E, CHI Instruments, Inc., Shanghai), using the anodized sample, Pt sheet and Ag/AgCl as the working, counter and reference electrodes, respectively. The electrolyte was prepared by dissolving 0.1 mol·L^{-1} $CuSO_4$ in a 3 mol·L^{-1} lactic acid solution, which pH was adjusted to 11.0 with 5.0 mol·L^{-1} NaOH solution. The electrolyte was stirred and kept at a constant temperature of 35 °C and a potential of − 0.8 V versus Ag/AgCl during the deposition process. The loadage of Cu was tailored by varying electrodeposition charges, i.e., 3, 6 and 8 mC (denoted as NP–3Cu, NP–6Cu and NP–8Cu, respectively). The samples were then ultrasonically washed with deionized water for 1 min followed by drying in air. For comparison, the Ni–Ti–O NPs (denoted as NP) were used as the control sample.

2.2 Sample characterization

Nano Measurer 1.2 software (Fudan University, China) was used to measure the pore size. Eighty pores were measured for each group. Field-emission scanning electron microscopy (FESEM, JSM-7001F, JEOL) with an accelerating voltage of 10 kV was performed to observe the surface and cross-sectional morphologies of the samples. The distribution of Ti, O, Ni and Cu along the longitudinal direction of the NPs was monitored by energy-dispersive X-ray spectroscopy (EDS, QX200, Bruker, Germany). Transmission electron microscopy (TEM, JEM-2100F, JEOL) was also performed to determine the microstructure of the NP–Cu.

2.3 Ni and Cu release

Each sample was immersed in 5 ml phosphate buffer saline (PBS) for 1 day at 37 °C; then, the PBS containing released Cu^{2+} and Ni^{2+} was collected and analyzed by inductively coupled plasma mass spectroscopy (ICP-MS, Agilent 7500, Agilent, America).

2.4 Antibacterial assay

The antibacterial properties of the samples against gram-positive *Staphylococcus aureus* (*S. aureus*, ATCC6538) were evaluated by plate-counting method [6]. All the samples were disinfected with 75% alcohol for 30 min and then washed with sterilized PBS before the antibacterial experiment. After *S. aureus* was shaking-cultured in a beef extract peptone (BEP, Sangon, China) medium at 37 °C for 12 h, the concentration of bacteria was diluted to 1×10^5 CFU·ml^{-1}, and then 1 ml of the suspension was introduced into each well of 24-well culture plate with sample and incubated at 37 °C for 12 h in darkness. At the end of incubation, the viable bacteria in the solution were quantified by standard serial dilution and plate-counting. The antibacterial rate was calculated using the following formula: $R = (B - A)/B \times 100\%$, where R means antibacterial ratio and B and A indicate the average number of viable bacteria in the bacterial suspension inoculated without and with the samples, respectively. Triple parallel samples were used in the experiment.

2.5 Cell culture

Bone marrow mesenchymal stem cells (BMSCs) were isolated from male Sprague Dawley (SD) rats aged 4–6 weeks. Briefly, the femur and tibia bone marrow of the rats were cut off and rinsed out using α-minimum essential medium (α-MEM, Gibco) containing 10% fetal bovine serum (FBS, Tianhang, China), 100 units·ml^{-1} penicillin

and 100 mg·ml^{-1} streptomycin. After that, the bone marrow extract was purified to culture. Cells at passages 2–3 were used for the experiments. The cells were cultured in α-MEM supplemented with 10% FBS, 100 units·ml^{-1} penicillin and 100 mg·ml^{-1} streptomycin in a cell incubator filled with 5% CO_2 at 37 °C. The culture medium was refreshed every other day. After the BMSCs were inoculated and cultured for 3 days, osteogenic induction medium (α-MEM with 10 mmol·L^{-1} β-glycerophosphate, 50 μg·ml^{-1} ascorbic acid and 1×10^{-8} mol·L^{-1} dexamethasone) was used to induce osteogenic differentiation. Triple parallel samples of each group were placed in the 24-well plates, sterilized by 75% alcohol for 45 min and then washed thrice with sterilized PBS before cell seeding.

2.6 Cell viability and proliferation

The cell viability of the BMSCs on different samples was evaluated by LIVE/DEAD® viability/cytotoxicity kit for mammalian cells (Invitrogen). Primarily, 1.5×10^4 cells·cm^{-2} were seeded onto each sample in a 24-well plate and cultured for 1, 4 and 7 days. At each time point, each sample was rinsed three times with PBS, followed by the injection of 50 μl working solution on each sample surface at 37 °C for 1 h in dark. Afterward, all the samples were rinsed with PBS and visualized using a confocal laser scanning microscope (CLSM, C2 Plus, Nikon, Japan).

3-(4,5-Dimethylthiazol-2-yl)-2, 5-diphenyltetrazolium bromide (MTT) assay was used to assess cell proliferation activity. The cells were cultured on each sample surface at a density of 1.5×10^4 cells·cm^{-2} for 1, 4 and 7 days. At the end of cultivation, all the samples were transferred to a new 24-well plate. Instantly, 100 μl of the MTT solution and 900 μl of the fresh culture medium were added to each well with sample and incubated at 37 °C for 4 h to form formazan. Subsequently, dimethyl sulfoxide (DMSO, Sangon, China) was used to dissolve the formazan. Finally, the absorbance of the resultant solution was measured at 492 nm on a microplate reader (Infinite F50, TECAN, Switzerland).

2.7 Alkaline phosphatase (ALP) activity

After being osteogenic induced for 3 and 7 days, the BMSCs (2×10^4 cells·cm^{-2}) cultured on the samples were fixed in 4% paraformaldehyde for 30 min, rinsed with PBS three times and stained with BCIP/NBT ALP Color Development Kit (Beyotime, China) according to the manufacturer's instructions to qualitatively assess the ALP activity.

2.8 Collagen secretion

Secretion of Type I collagen was assessed by Direct Red 80 staining method [7]. After induction culture for 7 and 14 days, the BMSCs (2×10^4 cells·cm^{-2}) on different substrates were fixed with 4% paraformaldehyde and stained using 0.1 wt% Direct Red 80 (Sigma, America) in aqueous saturated picric acid for 18 h. After that, the samples were rinsed with 0.1 mol·L^{-1} acetic acid to remove the redundant stain and the qualitative images were captured on an optical microscope (OM, DX70BD, SG). For quantitative assay, the stain on each sample surface was eluted with 1 ml fading solution (0.2 mol·L^{-1} NaOH/methanol 1:1) for 30 min and the absorbance was measured at 570 nm on the microplate reader. Three samples for each group were used in the experiment.

2.9 Extracellular matrix mineralization

Alizarin Red S (Sigma, America) staining was used to evaluate extracellular matrix (ECM) mineralization. After 7 and 14 days of culture with osteogenic induction medium, the cells (2×10^4 cells·cm^{-2}) seeded on each sample surface were fixed with 75% ethanol for 1 h and stained in 40 mmol·L^{-1} Alizarin Red S for 30 min at room temperature. Afterward, the samples were washed with distilled water again and again; then, the images of the samples were captured by an OM. In the quantitative analysis, the stain on the sample surfaces was eluted in 500 μl of 10% cetylpyridinium chloride (Sinopharm, China) in 10 mmol·L^{-1} sodium phosphate (Sinopharm, China) for 2 h and the optical density at 570 nm was then measured on the microplate reader. Three samples were used for each group.

2.10 Statistical analysis

All the experiments were done in triplicate, and the data from a typical experiment were shown. All statistical analysis was performed using the software SPSS 14.0 software. A one-way ANOVA followed by a Student–Newman–Keuls post hoc test was used to determine the level of significance. $p < 0.05$ was considered to be significant, and $p < 0.01$ was considered to be highly significant.

3 Results

3.1 Sample characterization

Figure 1a shows the surface morphology of samples. Nanoporous structure is formed on the sample surfaces,

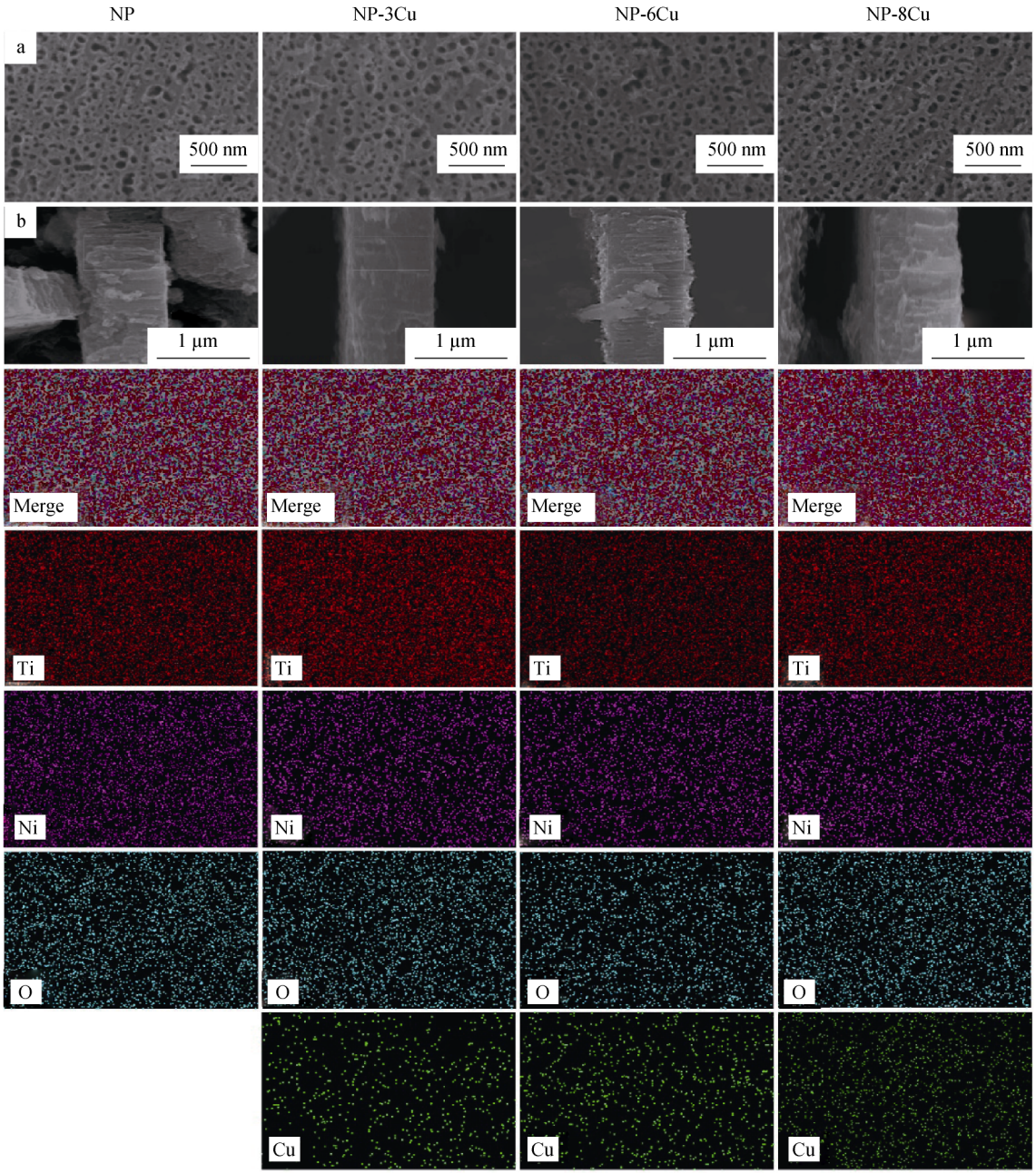

Fig. 1 **a** SEM images, **b** cross-sectional SEM images and corresponding elemental mapping images of NP, NP–3Cu, NP–6Cu and NP–8Cu samples

Table 1 Distribution of NP diameter measured by Nano Measurer 1.2 software (%)

Samples	30–45 nm	45–60 nm	60–75 nm	75–90 nm	90–105 nm
NP	2.50	30.00	41.25	21.25	5.00
NP–3Cu	3.75	26.25	38.75	25.00	6.25
NP–6Cu	8.75	22.50	35.00	28.75	5.00
NP–8Cu	10.00	28.75	37.50	16.25	7.50

and the pore diameter is mainly between 60 and 75 nm. The distributions of NP diameter are listed in Table 1. It is worth noting that the pore diameter does not alter after electrodeposition, which indicates that the deposition does not give rise to the change of surface morphology of the samples. The cross-sectional images in Fig. 1b indicate that the length of the samples is ~ 950 nm. Incorporation of Cu has little influence on the length. The distribution of Ni, Ti, O and Cu in the NPs along the longitudinal direction obtained by EDS elemental mapping is also shown in Fig. 1b. The images indicate that Ni, Ti, O and Cu are evenly distributed in the entire NPs. The atomic concentrations are listed in Table 2. With the increase in electrodeposition charges, the Cu concentration increases gradually. The microstructures of NP–8Cu were further investigated by TEM (Fig. 2). Nanoporous structure can be clearly seen in low-magnification image (Fig. 2a), and selected area electron diffraction (SAED) shows a dim halo, indicating its amorphous structure. High-magnification image (Fig. 2b) shows that black nanoparticles with diameter of about 2 nm are attached on the nanopore walls as indicated by red circles.

3.2 Ni and Cu ions release

The histogram of Ni and Cu ions release levels from different samples after immersion for 1 day is presented in Fig. 3. Clearly, the NP sample releases maximum Ni ions when compared with other groups. The release levels of Ni ions from NP–3Cu, NP–6Cu and NP–8Cu groups have no significant differences. The released Cu ion concentrations increase with electrodeposition charge.

3.3 Antibacterial ability

Figure 4 presents the antibacterial results of the samples. The optical images of plates in Fig. 4a show that the number of bacterial colonies of all the samples is less than that of blank control. With the increase in Cu content, the colony number decreases. Quantitative data in Fig. 4b show that the antibacterial rate increases with Cu content. Its value increases from 60% for NP to 93% for NP–8Cu.

Table 2 Elemental content of sample surfaces detected by EDS (at%)

Samples	Cu	Ni	Ti	O
NP	–	21.31	24.85	53.84
NP–3Cu	0.78	20.57	25.42	53.23
NP–6Cu	1.61	18.39	24.78	55.22
NP–8Cu	2.37	18.13	26.08	53.42

3.4 Cytotoxicity and cell proliferation

The cytotoxicity of the various samples is qualitatively determined by LIVE/DEAD viability/cytotoxicity kit after 1, 4 and 7 days of cultivation, and the results are presented in Fig. 5a. No dead cells can be seen on all the surface of the samples in the culture period, and the cell number increases with culture time, indicating that all the samples show good cytocompatibility. Quantitative assay by MTT (Fig. 5b) corroborates the qualitative results of the live/dead staining. It can be seen that the absorbance values increase with incubation time. There is no statistics difference in absorbance values between each group after culturing for 1 and 4 days. However, after culturing for 7 days, absorbance values of NP–3Cu and NP–6Cu are significantly higher than those of NP and NP–8Cu, which suggests that proper Cu content can promote cell proliferation.

3.5 Osteogenic differentiation

Osteogenic differentiation is evaluated by the ALP activity, collagen secretion and ECM mineralization of BMSCs. The early osteogenic differentiation is evaluated by ALP activity. The qualitative ALP activity after osteogenic induction for 3 and 7 days is shown in Fig. 6a. The ALP expression increases with prolonged osteogenic induction, whereas no significant difference can be observed from all the samples. The qualitative and quantitative results of collagen secretion of the BMSCs are shown in Fig. 6b, d; the amount of collagen secretion diminishes gradually with the increase in Cu content in the NPs after osteogenic induction for 7 days. However, after 14-day induction, the collagen amount on NP–6Cu is more than that on other samples. Figure 6c, e shows the qualitative and quantitative ECM mineralization results, respectively. After osteogenic induction for 7 and 14 days, NP–6Cu and NP–8Cu significantly enhance ECM mineralization compared to that of NP.

4 Discussion

Implant infection remains a major troublesome clinical complication. Incorporating antibacterial agents into the implant surface is a promising way to solve the problem. In this study, Cu-incorporated Ni–Ti–O NP coatings were prepared by anodization and electrodeposition to combine the favorable antibacterial ability of Cu and surface nanoporous structure to generate ideal biofunctionality.

Implant-associated infections are mainly caused by bacteria invasion, and once attaching firmly onto the implant surface, biofilms are formed, which can resist host

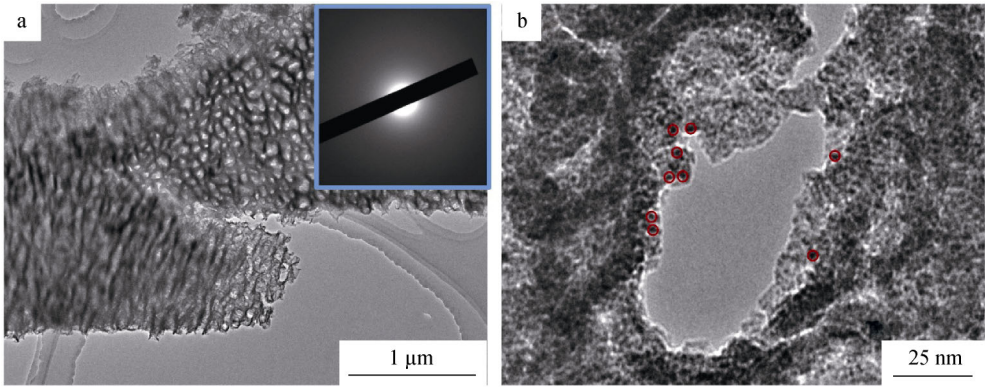

Fig. 2 TEM images of NP–8Cu at **a** low magnification and **b** high magnification (inset in **a** showing SAED pattern)

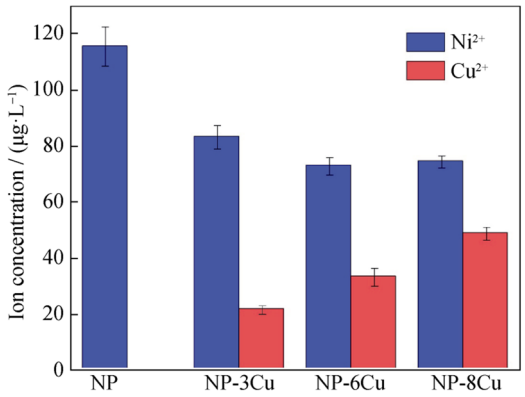

Fig. 3 Histogram of Ni and Cu ions release from samples

immune response [21]. Therefore, killing adjacent bacteria is the key to prevent implant-associated infections [22]. The number of bacteria in the culture medium decreases with Cu ion release amount, so Cu ion release plays a significant role in antibacterial ability. Cu ions can produce reactive oxygen species, damage respiratory enzymes and extract electrons from bacterial membranes, thereby resulting in cell lysis, cytoplasm leakage and bacteria death [23]. In addition, Ni ion release may also play a partial role. Compared with NP–Cu, NP sample releases more Ni^{2+}; it may be due to the addition of Cu. Some research has reported that Cu may suppress the anodic dissolution and thus also decrease the corrosion rate [24, 25].

It is widely accepted that Cu ions play a crucial role in the promotion of cell responses [26]. Thus, it is essential to control over the release amount of copper ions to avoid possible cytotoxicity [27]. Our experimental results show that the NP–Cu coatings are favorable for cell proliferation and even up-regulate collagen secretion and ECM mineralization. Moreover, numerous studies have suggested that NP shows good biocompatibility [28–30]. Cu ions are also reported to have similar effects [31, 32], namely a proper dose of Cu can significantly stimulate the differentiation and mineralization of BMSCs through up-regulating the

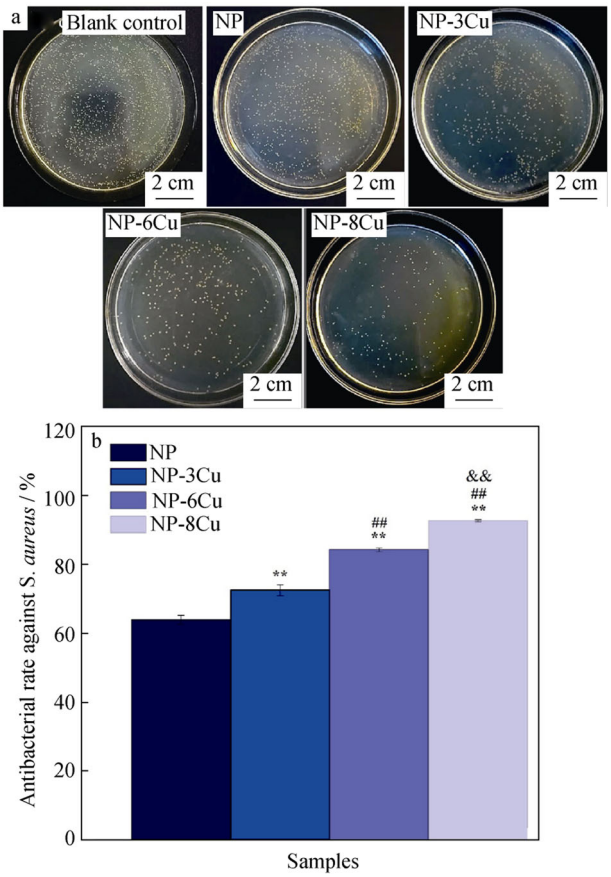

Fig. 4 **a** Optical photographs of *S. aureus* colonies on agar, which were previously extracted from the bacterial suspension inoculated with samples; **b** histogram of corresponding antibacterial rates ($^{**}p < 0.01$ compared to NP, $^{\#\#}p < 0.01$ compared to NP–3Cu, and $^{\&\&}p < 0.01$ compared to NP–6Cu)

expressions of bone-related genes, such as OPN, BMP-2 and Col-1. Similarly, in this work, as verified by the results of collagen synthesis and ECM mineralization, the NP–Cu coatings show better cytocompatibility after a prolonged period of incubation, which indicates the enhancement of Cu ion on BMSC osteogenic differentiation. This is

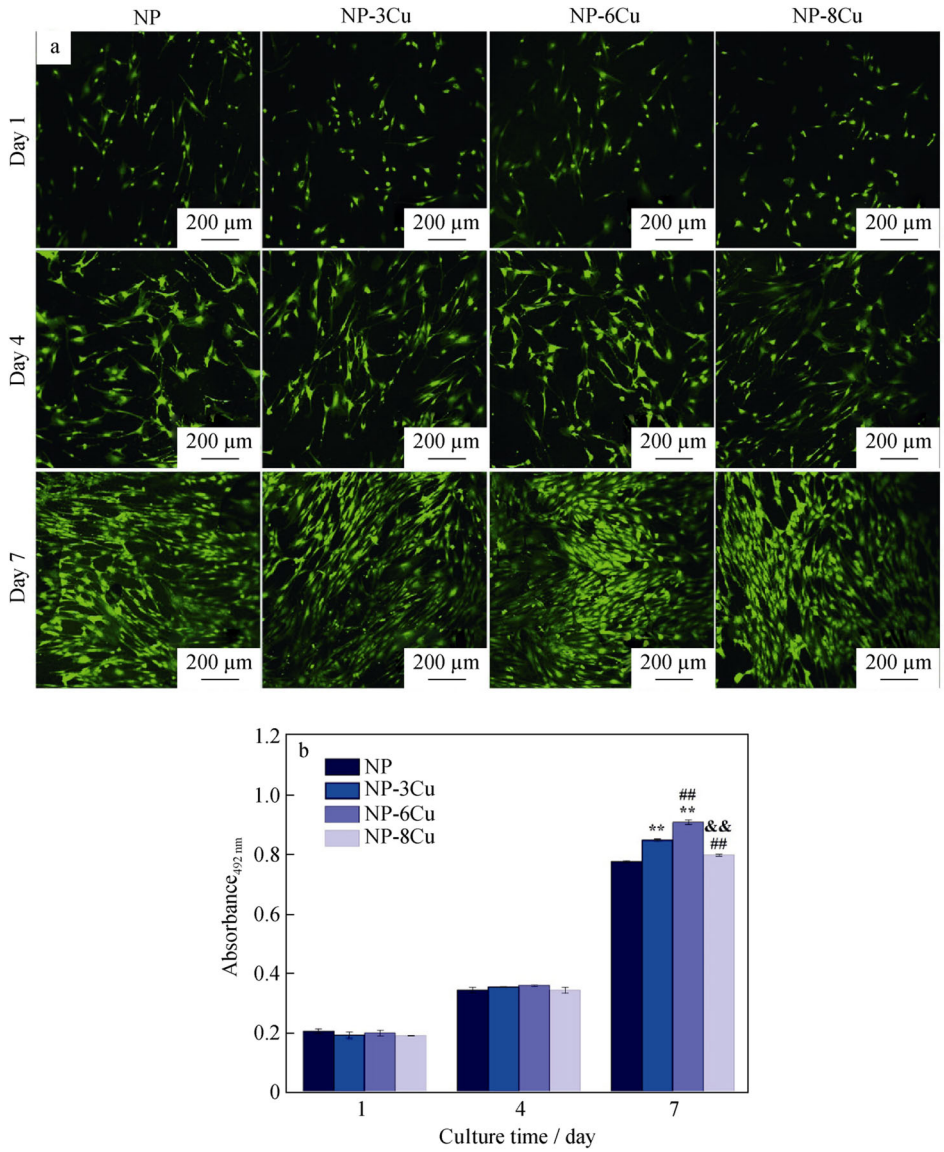

Fig. 5 **a** Fluorescence images with live/dead staining of BMSCs after culturing for 1, 4 and 7 days; **b** MTT results of BMSCs after culturing for 1, 4 and 7 days ($^{**}p < 0.01$ compared to NP, $^{\#\#}p < 0.01$ compared to NP–3Cu, and $^{\&\&}p < 0.01$ compared to NP–6Cu)

particularly important when the NiTi alloy serves as bone fixation implants to enhance bone healing.

Based on the results of the study, it seems to be a feasible and efficient method to incorporate Cu nutrient element into Ni–Ti–O NPs by electrodeposition. It still remains a serious challenge to develop desirable biological coatings on implant surfaces to increase the success rates of implant surgery. The prepared NP–Cu coatings in this work not only possess good antibacterial activity but also further facilitate cytocompatibility. Furthermore, we firmly believe that this work can provide a research foundation for further study of bioactive multifunctional coatings on the NiTi-based implant materials. Nonetheless, the present work only conducts in vitro experiments. Further in vivo studies are needed to prove the effectiveness of the coatings.

5 Conclusion

Ni–Ti–O NP coatings with different Cu contents were fabricated on biomedical NiTi alloy by anodization and electrodeposition. Electrodeposition has no influence on the morphology of the NPs. Cu ions are released from the coatings, which is responsible for their good antibacterial ability. Meanwhile, because of their controlled release, all the samples show better cytocompatibility and can even promote osteogenic differentiation of BMSCs. Favorable antibacterial ability and cytocompatibility render the coatings promising when serving as biomedical coatings of the NiTi alloy.

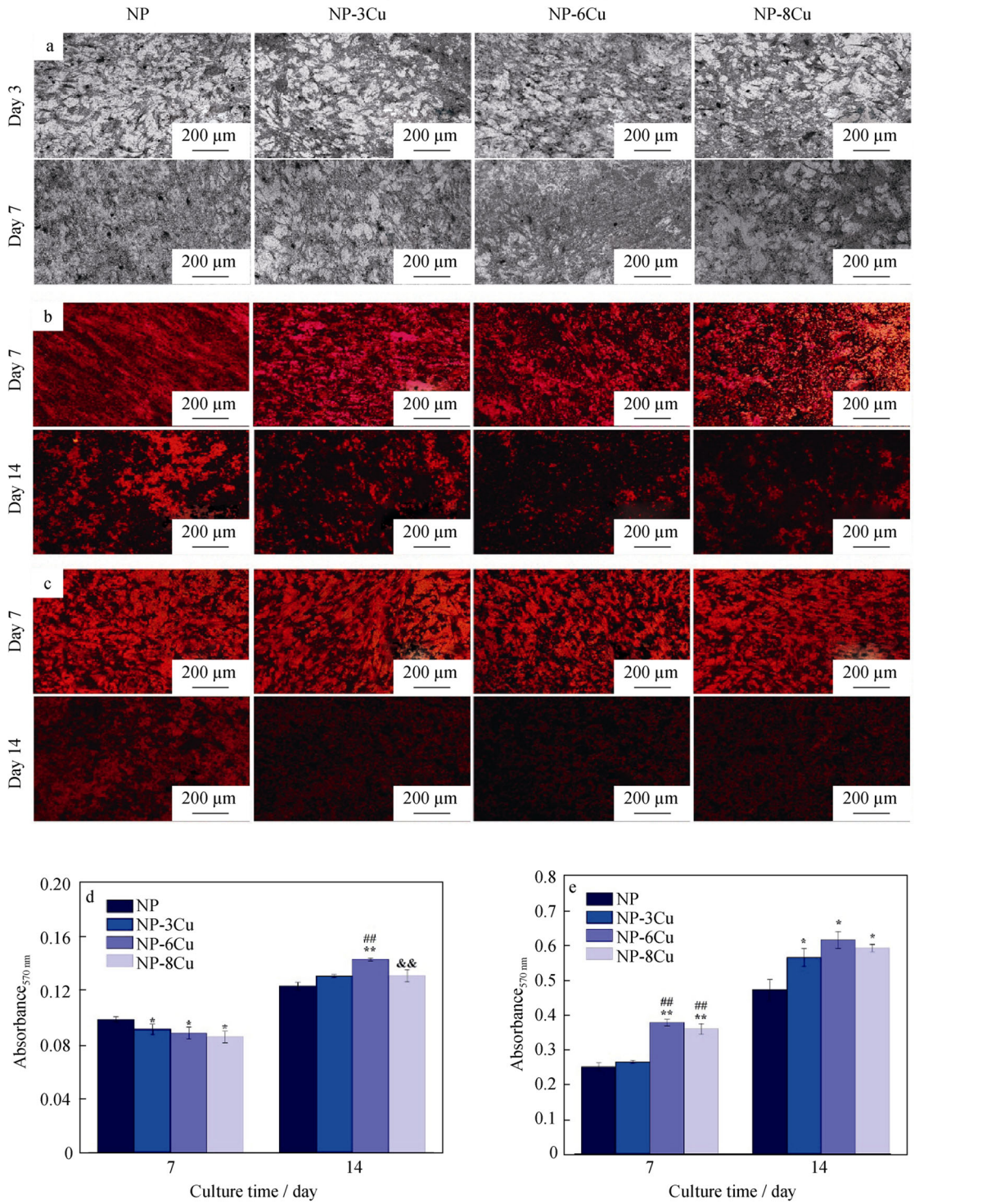

Fig. 6 **a** Qualitative images of ALP activity of BMSCs after osteogenic induction for 3 and 7 days; **b** qualitative images and **d** quantitative results of secretion level of Type I collagen from BMSCs after osteogenic induction for 7 and 14 days; **c** qualitative images and **e** quantitative results of ECM mineralization of BMSCs after osteogenic induction for 7 and 14 days ($^{*}p < 0.05$ and $^{**}p < 0.01$ compared to NP, $^{\#}p < 0.05$ and $^{\#\#}p < 0.01$ compared to NP–3Cu, and $^{\&}p < 0.05$ and $^{\&\&}p < 0.01$ compared to NP–6Cu)

Acknowledgements This work was financially supported by the Fund for Shanxi "1331 Project" Key Innovative Research Team (No. 1331KIRT), the Natural Science Foundation of Shanxi Province (No. 201801D121093) and the Key Innovative Research Team in Science and Technology of Shanxi Province (No. 201805D131001).

References

[1] Liu X, Wu S, Yeung KWK, Chan YL, Hu T, Xu Z, Liu X, Chung JCY, Cheung KMC, Chu PK. Relationship between osseointegration and superelastic biomechanics in porous NiTi scaffolds. Biomaterials. 2011;32(2):330.

[2] Wu S, Liu X, Yeung KWK, Guo H, Li P, Hu T, Chung CY, Chu PK. Surface nano-architectures and their effects on the mechanical properties and corrosion behavior of Ti-based orthopedic implants. Surf Coat Technol. 2013;233:13.

[3] Hang R, Zhang M, Ma S, Chu PK. Biological response of endothelial cells to diamond-like carbon-coated NiTi alloy. J Biomed Mater Res A. 2012;100(2):496.

[4] Liu Y, Ren Z, Bai L, Zong M, Gao A, Hang R, Jia H, Tang B, Chu PK. Relationship between Ni release and cytocompatibility of Ni–Ti–O nanotubes prepared on biomedical NiTi alloy. Corros Sci. 2017;123:209.

[5] Tan L, Li J, Liu X, Cui Z, Yang X, Zhu S, Li Z, Yuan X, Zheng Y, Yeung KW. Rapid biofilm eradication on bone implants using red phosphorus and near-infrared light. Adv Mater. 2018; 30(31):1801808.

[6] Chen Y, Gao A, Bai L, Wang Y, Wang X, Zhang X, Huang X, Hang R, Tang B, Chu PK. Antibacterial, osteogenic, and angiogenic activities of $SrTiO_3$ nanotubes embedded with Ag_2O nanoparticles. Mater Sci Eng C. 2017;75:1049.

[7] Gao A, Hang R, Huang X, Zhao L, Zhang X, Wang L, Tang B, Ma S, Chu PK. The effects of titania nanotubes with embedded silver oxide nanoparticles on bacteria and osteoblasts. Biomaterials. 2014;35(13):4223.

[8] Hang R, Liu Y, Bai L, Zhang X, Huang X, Jia H, Tang B. Length-dependent corrosion behavior, Ni^{2+} release, cytocompatibility, and antibacterial ability of Ni–Ti–O nanopores anodically grown on biomedical NiTi alloy. Mater Sci Eng C. 2018;89:1.

[9] Hang R, Liu Y, Bai L, Zong M, Wang X, Zhang X, Huang X, Tang B. Electrochemical synthesis, corrosion behavior and cytocompatibility of Ni–Ti–O nanopores on NiTi alloy. Mater Lett. 2017;202:5.

[10] Liu Y, Hang R, Zhao Y, Bai L, Sun Y, Yao X, Jia H, Tang B, Hang R. The effects of annealing temperature on corrosion behavior, Ni^{2+} release, cytocompatibility, and antibacterial ability of Ni–Ti–O nanopores on NiTi alloy. Surf Coat Technol. 2018;352:175.

[11] Denkhaus E, Salnikow K. Nickel essentiality, toxicity, and carcinogenicity. Crit Rev Oncol Hematol. 2002;42(1):35.

[12] Bai L, Hang R, Gao A, Zhang X, Huang X, Wang Y, Tang B, Zhao L, Chu PK. Nanostructured titanium–silver coatings with good antibacterial activity and cytocompatibility fabricated by one-step magnetron sputtering. Appl Surf Sci. 2015;355:32.

[13] Xu Z, Li M, Li X, Liu X, Ma F, Wu S, Yeung K, Han Y, Chu PK. Antibacterial activity of silver doped titanate nanowires on Ti implants. ACS Appl Mater Interfaces. 2016;8(26):16584.

[14] Zong M, Bai L, Liu Y, Wang X, Zhang X, Huang X, Hang R, Tang B. Antibacterial ability and angiogenic activity of Cu–Ti–O nanotube arrays. Mater Sci Eng C. 2017;71:93.

[15] Hang R, Gao A, Huang X, Wang X, Zhang X, Qin L, Tang B. Antibacterial activity and cytocompatibility of Cu–Ti–O nanotubes. J Biomed Mater Res A. 2014;102(6):1850.

[16] Wang L, Ren Y, Qin G. Research progress of Zn-based alloys as biodegradable materials. Chin J Rare Metals. 2017;41(5):571.

[17] Zhang K, Zhu Y, Liu X, Cui Z, Yang X, Yeung KWK, Pan H, Wu S. Sr/ZnO doped titania nanotube array: an effective surface system with excellent osteoinductivity and self-antibacterial activity. Mater Des. 2017;130:403.

[18] Kalaivani S, Singh RK, Ganesan V, Kannan S. Effect of copper (Cu^{2+}) inclusion on the bioactivity and antibacterial behavior of calcium silicate coatings on titanium metal. J Mater Chem B. 2014;2(7):846.

[19] Matsumoto N, Sato K, Yoshida K, Hashimoto K, Toda Y. Preparation and characterization of β-tricalcium phosphate co-doped with monovalent and divalent antibacterial metal ions. Acta Biomater. 2009;5(8):3157.

[20] Zhao D-P, Tang J-C, Nie H-M, Zhang Y, Chen Y-K, Zhang X, Li H-X, Yan M. Macro-micron-nano-featured surface topography of Ti–6Al–4V alloy for biomedical applications. Rare Met. 2018;37(12):1055.

[21] Huang R, Han Y, Lu S. Enhanced osteoblast functions and bactericidal effect of Ca and Ag dual-ion implanted surface layers on nanograined titanium alloys. J Mater Chem B. 2014; 2(28):4531.

[22] Necula BS, van Leeuwen JP, Fratila-Apachitei LE, Zaat SA, Apachitei I, Duszczyk J. In vitro cytotoxicity evaluation of porous TiO_2–Ag antibacterial coatings for human fetal osteoblasts. Acta Biomater. 2012;8(11):4191.

[23] Sharifahmadian O, Salimijazi HR, Fathi MH, Mostaghimi J, Pershin L. Relationship between surface properties and antibacterial behavior of wire arc spray copper coatings. Surf Coat Technol. 2013;233:74.

[24] Xi T, Shahzad MB, Xu D, Sun Z, Zhao J, Yang C, Qi M, Yang K. Effect of copper addition on mechanical properties, corrosion resistance and antibacterial property of 316L stainless steel. Mater Sci Eng C. 2017;71:1079.

[25] Wu H, Zhang X, He X, Li M, Huang X, Hang R, Tang B. Wear and corrosion resistance of anti-bacterial Ti–Cu–N coatings on titanium implants. Appl Surf Sci. 2014;317:614.

[26] Matos L, Gouveia A, Almeida H. Copper ability to induce premature senescence in human fibroblasts. Age. 2012;34(4): 783.

[27] Burghardt I, Luthen F, Prinz C, Kreikemeyer B, Zietz C, Neumann HG, Rychly J. A dual function of copper in designing regenerative implants. Biomaterials. 2015;44:36.

[28] Rodriguez-Contreras A, Bello DG, Nanci A. Surface nanoporosity has a greater influence on osteogenic and bacterial cell adhesion than crystallinity and wettability. Appl Surf Sci. 2018;445:255.

[29] Gulati K, Moon HJ, Li T, Sudheesh Kumar PT, Ivanovski S. Titania nanopores with dual micro-/nano-topography for selective cellular bioactivity. Mater Sci Eng C. 2018;91:624.

[30] Bello DG, Fouillen A, Badia A, Nanci A. A nanoporous titanium surface promotes the maturation of focal adhesions and formation of filopodia with distinctive nanoscale protrusions by osteogenic cells. Acta Biomater. 2017;60:339.

[31] Wu Q, Li J, Zhang W, Qian H, She W, Pan H, Wen J, Zhang X, Liu X, Jiang X. Antibacterial property, angiogenic and osteogenic activity of Cu-incorporated TiO_2 coating. J Mater Chem B. 2014;2(39):6738.

[32] Huang X, Liu Y, Yu H, Yang X, Wang Y, Hang R, Tang B. One-step fabrication of cytocompatible micro/nano-textured surface with TiO_2 mesoporous arrays on titanium by high current anodization. Electrochim Acta. 2016;199:116.